Article

Novel Push–Pull Dyes Derived from 1*H*-cyclopenta[*b*]naphthalene-1,3(2*H*)-dione as Versatile Photoinitiators for Photopolymerization and Their Related Applications: 3D Printing and Fabrication of Photocomposites

Ke Sun [1,2], Shaohui Liu [1,2], Corentin Pigot [3] , Damien Brunel [3] , Bernadette Graff [1,2], Malek Nechab [3] , Didier Gigmes [3] , Fabrice Morlet-Savary [1,2], Yijun Zhang [1,2], Pu Xiao [4,*], Frédéric Dumur [3,*] and Jacques Lalevée [1,2,*]

[1] Université de Haute-Alsace, CNRS, IS2M UMR 7361, F-68100 Mulhouse, France; ke.sun@uha.fr (K.S.); shaohui.liu@uha.fr (S.L.); bernadette.graff@uha.fr (B.G.); fabrice.morlet-savary@uha.fr (F.M.-S.); yijun.zhang@uha.fr (Y.Z.)

[2] Université de Strasbourg, F-67081 Strasbourg, France

[3] Aix Marseille Univ, CNRS, ICR UMR 7273, F-13397 Marseille, France; pigotcorentin2@gmail.com (C.P.); damien.brunel@univ-amu.fr (D.B.); malek.nechab@univ-amu.fr (M.N.); didier.gigmes@univ-amu.fr (D.G.)

[4] Research School of Chemistry, Australian National University, Canberra ACT 2601, Australia

[*] Correspondence: pu.xiao@anu.edu.au (P.X.); frederic.dumur@univ-amu.fr (F.D.); jacques.lalevee@uha.fr (J.L.)

![check for updates logo] check for updates

Abstract: A series of eleven push–pull chromophores with specific structures have been designed for the free radical polymerization of acrylates, but also for the fabrication of photocomposites and 3D-printed structures. New photoinitiating systems comprising the different push–pull dyes showed excellent photochemical reactivities at 405 nm. Notably, polymerization reactions could be initiated with light-emitting diodes (LEDs) which constitute a unique opportunity to promote the free radical polymerization under mild conditions, i.e., low light intensity (e.g., *sunlight*) and under air. Photopolymerization is an active research field, and push–pull dyes have already been investigated for this purpose. Besides, it remains of crucial interest to investigate new reactive structures capable of efficiently initiating photopolymerization reactions. The plausible potential of these structures to act as efficient photoinitiators in vat photopolymerization (or 3D printing) and fabrication of photocomposites prompts us to select eleven new push–pull dyes to design multi-component photoinitiating systems activable with LEDs emitting at 405 nm. Precisely, a tertiary amine, i.e., ethyl dimethylaminobenzoate (EDB) used as an electron/hydrogen donor and an iodonium salt used as an electron acceptor were selected to behave as powerful co-initiators to construct three-component photoinitiating systems (PISs) with the different push–pull dyes. Among these new PISs, dye **8** and **9**-based PISs could efficiently promote the free radical photopolymerization of acrylates upon exposure to a LED emitting at 405 nm also upon sunlight irradiation, highlighting their huge performance. Photoinitiating abilities could be explained on the basis of steady state photolysis experiments. Fluorescence measurements and electron spin resonance (ESR) spin-trapping experiments were also performed to obtain a deeper insight into the chemical mechanisms supporting the polymerization reaction and determine the way the initiating species, i.e., the radicals, are observed. Finally, two investigated dye-based PISs were applied to the fabrications of photocomposites. Three-dimensional patterns with excellent spatial resolutions were generated by the laser writing technique to identify the effects of photopolymerization of acrylates both in the absence and presence of fillers (silica). Interestingly, comparison between the 3D objects

fabricated by the PISs/monomer systems and the PISs/monomer/filler photocomposites indicates that the newly designed photocomposites are suitable for practical applications.

1. Introduction

Push–pull dyes composed of a donor and an acceptor connected by mean of a conjugated spacer have been the focus of intense research efforts due to the wide range of applications in which these dyes can find applications [1–5]. Among them, organic electronics, including organic photovoltaics (OPVs) [6,7], organic light-emitting diodes (OLEDs) [8], organic-field effects transistors (OFETs) [9] but also nonlinear optics (NLO) [10–16], water waste treatment [17] or the design of organic probes for diagnostics or bioimaging [18,19], can be cited as a popular research field. By separating the electron-donating group from the electron-accepting group, a strong electronic delocalization can be induced, furnishing molecules with high molar extinction coefficients and displaying a strong absorption band in the visible range corresponding to the intramolecular charge transfer (ICT) band [20–24]. By finely tuning both the electron-donating and electron-accepting abilities of the two partners as well as on the length of the spacer, the molar extinction coefficients but also the position of the ICT band can be carefully controlled [2]. Benefiting from these different advantages (high molar extinction coefficient, absorption in the visible range), push–pull dyes have thus been identified as promising candidates for the design of visible light photoinitiators activable under low-light intensity [25–28].

However, the design of highly reactive dyes capable of initiating photopolymerization processes under light emitted by 405 nm LEDs are still scarcely available in the literature, and a great deal of efforts remains to be carried out in order to develop photoinitiators operating under very low-light intensities [29–33]. Such a goal can only be achieved by chemical engineering. Fortunately, this obstacle can be easily overcome by extending the polyaromaticity of the electron-accepting group [2,34]. To illustrate this, the remarkable work conducted on a series of push–pull dyes comprising indane-1,3-dione or its extended version, i.e., 1*H*-cyclopentanaphthalene-1,3-dione as the electron accepting groups, has clearly evidenced the advantage of this strategy, with a redshift of the absorption spectra as well as an enhancement of the molar extinction coefficient for the 1*H*-cyclopenta naphthalene-1,3-dione-based dyes. As a result of this, 1*H*-cyclopentanaphthalene-1,3-dione-based dyes showed improved photoinitiating abilities compared to the indane-1,3-dione-based dyes [35]. Aiming at improving the knowledge of photopolymerization, the fabrication of novel useful photocomposites by use of push–pull dyes as photoinitiators and in the presence of fillers was considered by our group as one of the various useful applications which is only scarcely reported in the literature [36].

In the present study, the design of push–pull dyes based three-component photoinitiating systems both for 3D printing and composites preparation under mild conditions, e.g., room temperature and 405 nm LED irradiation, is reported (See Scheme 1). Eleven dyes have been selected and examined for the first time as photoinitiators when combined with an iodonium salt (Speedcure 938) and an amine (EDB) for the free radical polymerization of acrylates (See Figure 1). Interestingly, two dyes with 3-(dialkyl amino)-1,2-dihydro-9-oxo-9*H*-indeno [2,1-*c*]pyridine-4-carbonitrile group showed high final monomer conversions and impressive photoinitiation abilities, what was investigated by real-time Fourier transform Infrared spectroscopy (RT-FTIR) upon irradiation at 405 nm with a LED. Parallel to the polymerization tests carried out with LEDs of well-defined emissions, sunlight-induced photopolymerization was also investigated, paving the way towards greener polymerization processes. In order to compare the photoinitiating abilities of the different dyes, their optical properties were characterized by UV–visible absorption spectroscopy. Photolysis experiments were also carried out

to compare their photochemical interactions with the different additives. Moreover, the two most remarkable dyes (i.e., dyes **8** and **9**) were selected to perform fluorescence quenching and ESR spin experiments in order to determine the exact chemical mechanisms supporting the generation of free radicals. Electrochemical properties as well as the way to produce free radical are also discussed. Particularly, with such a high photoreactivity, the new proposed systems can be used for sunlight induced polymerization as an example of green and mild conditions. Finally, 3D printing experiments were carried out with trimethylolpropane triacrylate (TMPTA) as the acrylate monomer, and making use of the newly proposed photoinitiating systems, photocomposites (TMPTA/silica) could be prepared. As expected, 3D patterns with a remarkable resolution were successfully prepared.
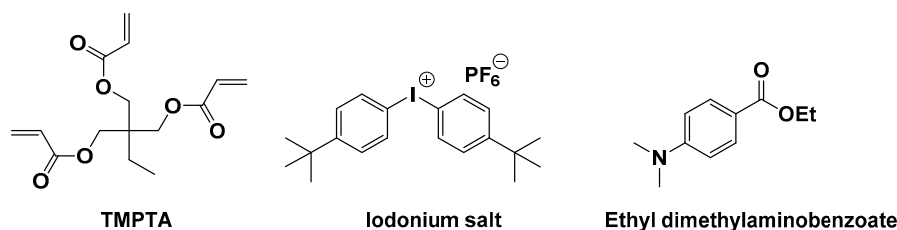
Scheme 1. Chemical structures of the iodonium salt, the tertiary amine and the trifunctional acrylate monomer.

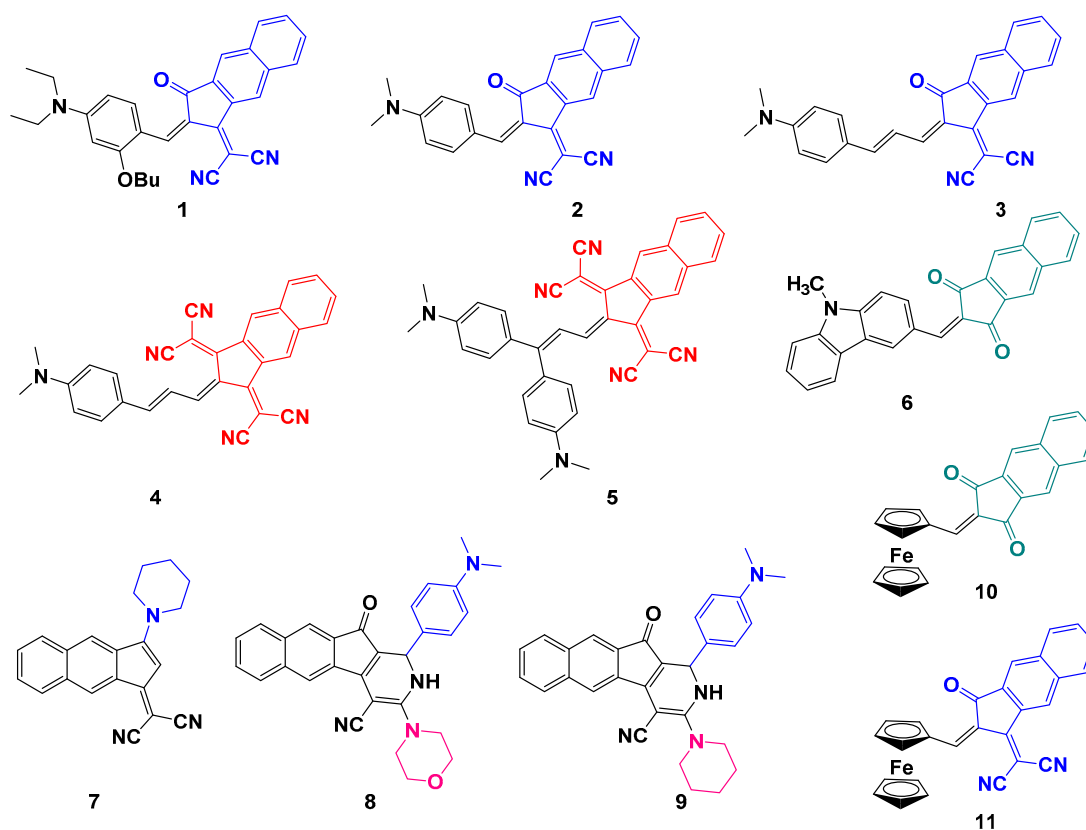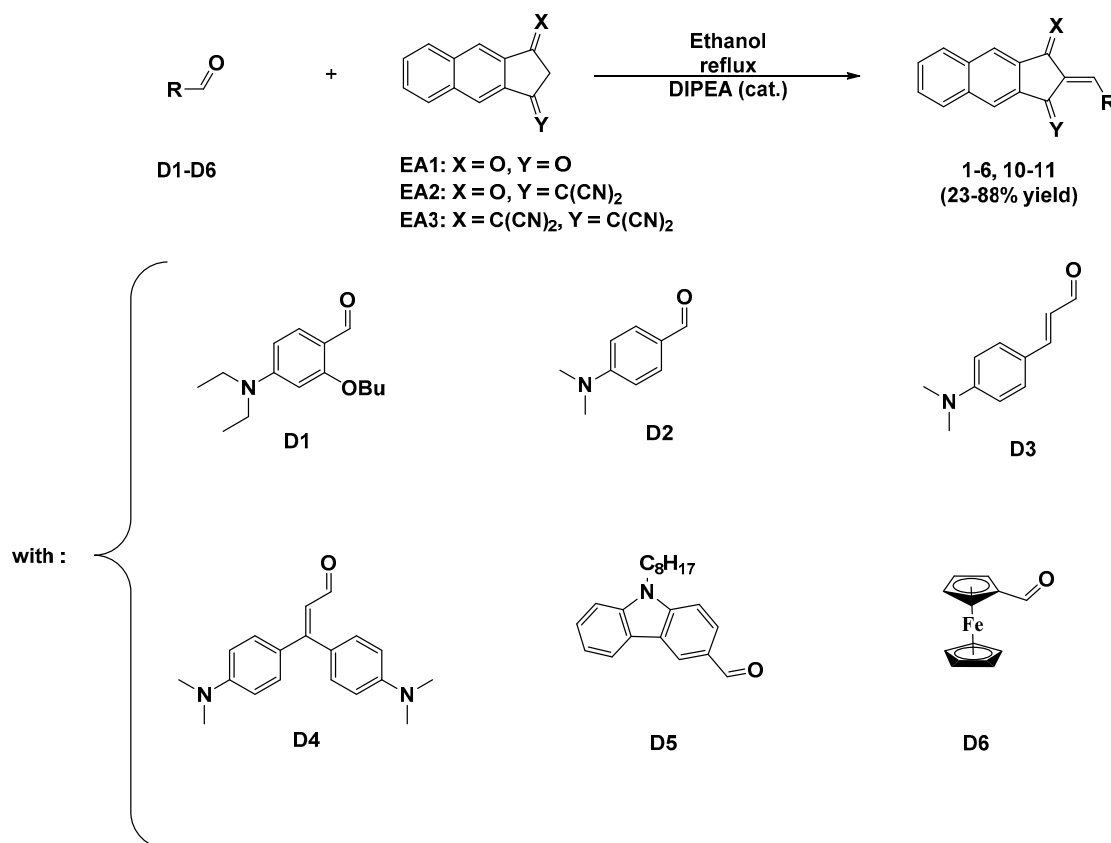**Figure 1.** Chemical structures of dyes **1**–**11**.

2. Results

2.1. Synthesis of the Different Dyes

　　With aim at developing push–pull dyes with high molar extinction coefficients and broad absorption spectra extending over the visible range, two synthetic approaches were employed. The first one consisted of extending the aromaticity of the electron acceptor by replacing the phenyl group of the

well-established indane-1,3-dione by a naphthalene group (See Scheme 2, **EA1**) or by using electron donors with an elongated π-conjugated system (See Scheme 2, **D3/D4**). **EA1** can be synthesized with 91% yield by a two-step synthesis including a Claisen condensation followed by a decarboxylation of the intermediary sodium salt (See Scheme 3) [4].

EA1: X = O, Y = O
EA2: X = O, Y = C(CN)$_2$
EA3: X = C(CN)$_2$, Y = C(CN)$_2$

1-6, 10-11
(23-88% yield)

D1-D6

with :

D1   D2   D3

D4   D5   D6

Scheme 2. Synthetic pathways to dyes **1–6** and dyes **10,11** and the six aldehydes, **D1–D6**, used in this study.
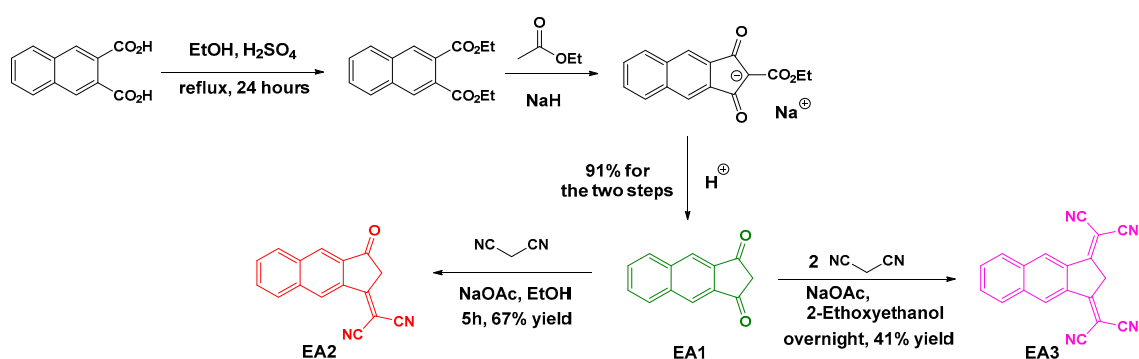
Scheme 3. Synthetic routes to building blocks **EA1, EA2 and EA3**.

The second approach consisted of improving the electron accepting properties of the electron acceptor used in the push–pull molecules. In the case of indane-1,3-dione derivatives, addition of malononitrile has been identified as one of the most efficient approach to achieve this goal. Indeed, the Knoevenagel condensation is a convenient strategy to add selectively one or two cyano groups onto the indane-1,3-dione moiety. This strategy also has the advantage of extending the length of the π-conjugated system in the electron-accepting moiety (See Figure 1).

Nevertheless, few examples of introducing malononitrile onto naphthalene-1,3-dione have been reported. Indeed, we have noticed a much lower reactivity of the molecule compare to the classical indane-1,3-dione, leading to longer reaction times to prepare for the dicyanovinyl derivative **EA2**. To prepare the tetracyano derivative, a change in the solvent used to perform the reaction was even required in order to reach a higher reaction temperature and introduce a second dicyano group. By use of 2-ethoxyethanol, **EA3** could be prepared in 41% yield. This difference of reactivity is probably attributable to the high stability of the intermediate **EA2** anion in basic medium, adversely affecting the second Knoevenagel reaction used to introduce the second dicyano group.

The Knoevenagel condensation reaction enables the production of the push–pull dyes in short reaction times, and being an easy-to-handle reaction, this condensation has been selected as the appropriate reaction to synthetize the molecules **1–6** and **10–11**. Despite the fact that piperidine, a usual and cheap organocatalyst, was used to perform this reaction, we observed during the synthesis of **3** the undesired formation of dye **7** by nucleophilic addition of piperidine [5]. Similarly, during the synthesis of dye **2**, we also noticed the undesired intramolecular cyclization (Dye **9**) similar to that reported by Landmesser et al. (See Scheme 4) [37].
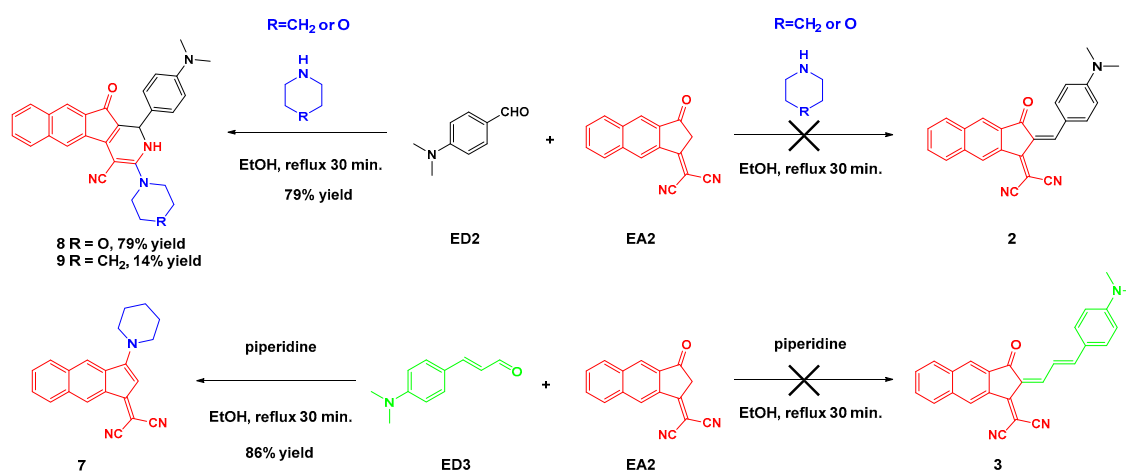
Scheme 4. Synthesis of dye **7** with **ED3** acting as the organocatalyst (bottom) and synthesis of the azafluorenone adducts (dyes **8** and **9**) when using **EA2**, **ED2** and a secondary base, such as morpholine or piperidine.

This cyclization reaction is notably observed when nucleophilic amines such as piperidine are used. Considering that no formation of azafluorenones by cyclization reaction was reported in the literature with 2-(3-oxo-2,3-dihydro-1*H*-cyclopenta[*b*]naphthalen-1-ylidene)malononitrile (**EA2**) as the electron acceptor, we notably pursued this study by replacing piperidine by morpholine, giving rise to the same cyclization reaction and furnishing dye **8** in 79% yield. Considering that nucleophilic amines can add onto the electron accepting moiety of the push–pull dye and initiate a cyclization reaction (See Scheme 4), piperidine was replaced by the none-nucleophilic base *N,N*-diisopropylethylamine (DIPEA) for the synthesis of dyes **1,2,3** and **11**, as shown in the Scheme 1. Concerning the ferrocene adducts **10** and **11**, it has to be noticed that a lower reaction yield was obtained for dye **11** (23% yield) than for dye **10** (88% yield), which can be assigned to the steric hindrance of DIPEA, adversely affecting its catalyst activity when a bulky electron donor such as ferrocene is used.

2.2. Photopolymerization Kinetics for Newly Push–Pull Dyes in Three-Component Photoinitiating Systems

Photoinitiation abilities of the eleven dyes-based PISs (from dye **1** to **11**) were investigated by infrared spectroscopy (RT-FTIR) while irradiating the resins with a LED@405 nm ($I_0 = 110$ mW cm^{-2}) for 400 s at room temperature. Typical acrylate function conversions vs. irradiation time profiles are depicted in Figure 2. In order to evidence their better photoinitiation abilities, the specific curve 0

was given for photopolymerization of acrylate monomer TMPTA initiated by two-component PIS (2% Iod: 2% Amine in 1 g TMPTA) without dyes. Obviously, the profiles indicate that the dye-based three-component PISs are remarkable combinations to initiate the free radical photopolymerization of acrylates when compared with the Iod/amine two-component system as shown in Figure 2. However, the polymerization processes initiated by the three-component systems comprising dyes **4**, **10** and **11** are less efficient than the Iod/amine system (curve 0). Thus, it is convincing that push–pull chromophores with ferrocene groups can only hardly work as efficient photoinitiators in free radical polymerization processes. In the case of dyes **5, 7, 8** and **9**, the highest final monomer conversions and the fastest conversions were obtained with these four dyes, which proved to efficiently promote the photopolymerization of TMPTA. For instance, the highest final reactive function conversions (FCs) were attained with dye **8** (beyond 90%), as well as dyes **5, 7, 9**, which also furnished high final acrylate function conversions beyond 80%. The short conversion times within 50 s also evidenced their high photoinitiation abilities as well. Excellent polymerization profiles could also be determined with the other dyes, e.g., dyes **1, 2, 3, 6**, which showed slightly lower performances (the FCs attained for the free radical polymerization (FRP) of TMPTA were about 70%~80%) during free radical photopolymerization processes, except for the four dyes mentioned above.
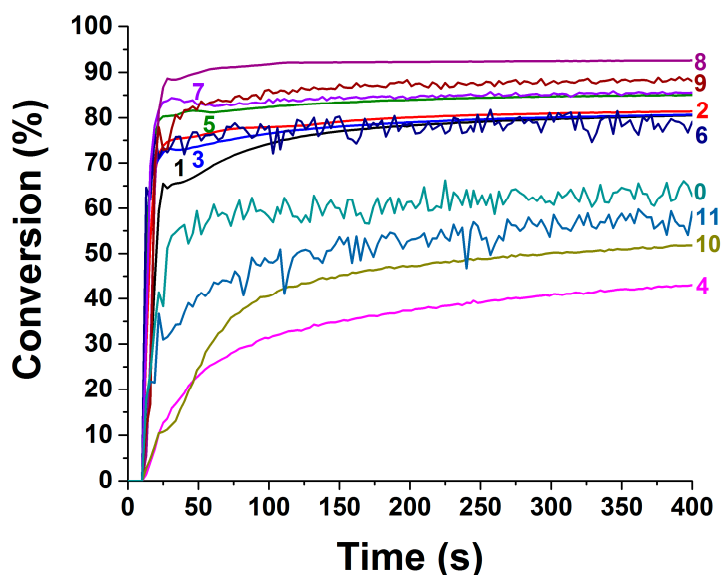

Figure 2. Photopolymerization profiles of TMPTA (conversion rate of C=C bonds vs. irradiation time) initiated by iodonium and amine (ethyl dimethylaminobenzoate, EDB) upon exposure to a LED@405 nm under air in the presence of dyes **1–11** at the same weight ratio: dye: iodonium salt (Speedcure 938): Speedcure EDB = 0.1%:2%:2% in 1 g TMPTA. Curve 0 corresponds to the initiating system (iodonium/amine) without dye.

To investigate the photopolymerization kinetics more precisely and specifically, the highest final reactive function conversions (FCs) concerning the polymerization of TMPTA in the presence of all eleven dyes are gathered in Table 1. From the different experiments, a comparison of the FCs obtained with the eight most reactive dyes could be established, and the following order of reactivity could be deduced: dye **8** > dye **9** > dye **7** > dye **5** > dye **2** > dye **3** (or dye **1**) > dye **6**. Interestingly, dyes **8, 9** have similar chemical structures, but their light absorption properties are much lower than those of the other dyes, e.g., dye **1** and dye **6** (See Figure 1). Light absorption properties of the push–pull dyes will be discussed in the following part.

Table 1. Final acrylate function conversions (FCs) obtained upon irradiation at 405 nm for TMPTA using three-component photoinitiating systems: dyes/iodonium salt/amine (0.1%, 2%/2%, w/w) and the concentration of the different dyes in resins.

Dye	0 (Blank) [a]	1	2	3	4	5
FCs	60%	78%	80%	78%	43%	84%
[dye]	0	2.31×10^{-3}	2.93×10^{-3}	2.74×10^{-3}	2.44×10^{-3}	1.93×10^{-3}
Dye	**6**	**7**	**8**	**9**	**10**	**11**
FCs	76%	85%	91%	88%	51%	56%
[dye]	2.84×10^{-3}	3.53×10^{-3}	2.38×10^{-3}	2.39×10^{-3}	2.80×10^{-3}	2.50×10^{-3}

[a]: iodonium salt/amine (2%/2%, w/w) without dye.

2.3. Photopolymerization Kinetics upon Exposure to Sunlight for Push–Pull Dye 8

Photoinitiation abilities of dye **8**-based PIS were also investigated using Fourier transform infrared spectroscopy (FT-IR) under sunlight irradiation (Mulhouse, France) as a very good example of mild irradiation conditions. Moreover, typical acrylate function conversions vs. irradiation time (in 0, 10, 20, 30 min) were extracted from the decrease in the peak at 6130 cm^{-1}. As shown in Figure 3, the polymerization profile indicates the acrylate function conversion reached at ~88%, which demonstrates that dye-based three-component PISs can be photoinitiated by sunlight. Remarkably, the free radical polymerization is promoted to a high level of conversion (~88%) with sunlight when compared with the photopolymerization obtained at 405 nm (I_0 = 110 mW cm^{-2}) (91% conversion). To conclude, by carefully selecting the push–pull dyes with excellent performance, high-performance photoinitiating systems activable under mild irradiations, e.g., 405 nm LED (I_0 = 110 mW cm^{-2}), or under sunlight ($I_0 < 5$ mW cm^{-2} in the 350–500 nm range) have thus been proposed in this work.
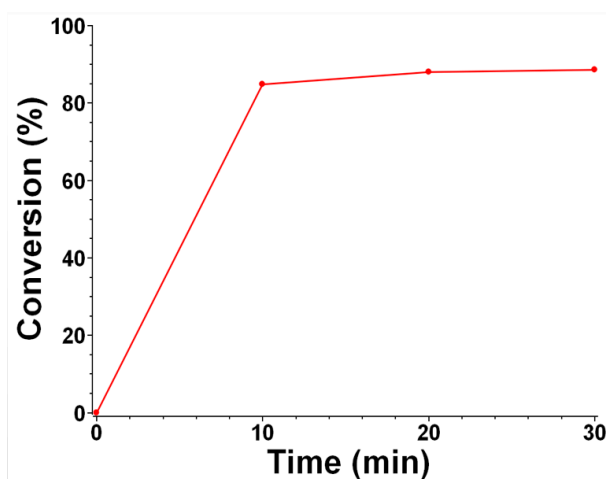

Figure 3. Conversion of C=C bond using the dye **8**/iodonium/amine system vs. sunlight irradiation time (0 min, 10 min, 20 min, 30 min).

3. Discussion

3.1. Light Absorption Properties of the Push–Pull Dyes

Molar extinction coefficients of the different dyes were determined by UV–visible absorption spectroscopy in acetonitrile (see Figure 4), and the light absorption parameters are gathered in Table 2. Dyes **1**, **2**, **3**, **5**, **6** showed very high molar extinction coefficients, e.g., ε(Dye **1**) = 38,580 M^{-1} cm^{-1} at λ_{max} = 601 nm, ε(Dye **2**) = 24,872 M^{-1} cm^{-1} at λ_{max} = 582 nm. ε(Dye **3**) = 16,330 M^{-1} cm^{-1} at λ_{max} = 661 nm, ε(Dye **5**) = 22,990 M^{-1} cm^{-1} at λ_{max} = 727 nm, and ε(Dye **6**) = 49,650 M^{-1} cm^{-1} at λ_{max} = 447 nm, in the UV–visible range, which fit well to their relatively high photoinitiation abilities

mentioned above. Interestingly, dyes **7**, **8**, **9** showed both low molar extinction coefficients at λ_{max} and at 405 nm compared to dyes **1**, **2**, **3**, **5**, **6**. However, their performances on photopolymerization are much better. As expected, the lower maximum extinction coefficients of dyes **10** and **11** led to poor photoinitiation abilities as well.
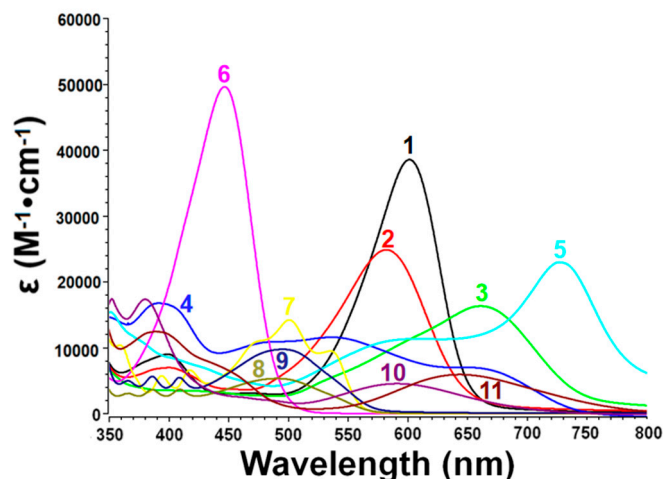

Figure 4. UV–visible absorption spectra in acetonitrile of the push–pull dyes (dyes **1–11**) in acetonitrile.

Table 2. Photophysical properties of the different push–pull dyes in acetonitrile: maximum absorption wavelengths λ_{max}; molar extinction coefficients at λ_{max} (ε_{max}); and molar extinction coefficients at 405 nm ($\varepsilon_{405\,nm}$).

	λ_{max} (nm)	ε_{max} (M^{-1} cm^{-1})	$\varepsilon_{@405nm}$ (M^{-1} cm^{-1})
Dye **1**	601	38,580	8560
Dye **2**	582	24,872	6870
Dye **3**	661	16,330	3500
Dye **4**	537	11,600	16,090
Dye **5**	727	22,990	8320
Dye **6**	447	49,650	22,910
Dye **7**	500	14,220	3880
Dye **8**	491	5330	3340
Dye **9**	495	9763	4950
Dye **10**	591	4550	8630
Dye **11**	644	5930	11,348

3.2. Optical Properties of Dyes 8 and 9

To demonstrate the contribution of the 3-(dialkylamino)-1,2-dihydro-9-oxo-9*H*-indeno[2,1-*c*] pyridine-4-carbonitrile group on the photopolymerization process, photolysis experiments were carried out in acetonitrile at 405 nm with dyes **8** and **9** in the presence of Iod and EDB. The same light intensity (LED@405 nm, $I_0 = 110$ mW cm^{-2}) than that used for photopolymerization was employed for the different experiments reported in this section. As shown in the UV–visible absorption spectra depicted in Figure 5a, a clear photolysis in solution was observed for the dye **8**-based three-component photoinitiating systems. Parallel to this, the two-component dye **8**/EDB system also showed an efficient photolysis (See Figure 5c), which was in agreement with the extinction coefficient of dye **8** at the emission wavelength of the LED@405 nm ($\varepsilon_{@405nm} = 3340$ M^{-1} cm^{-1}).
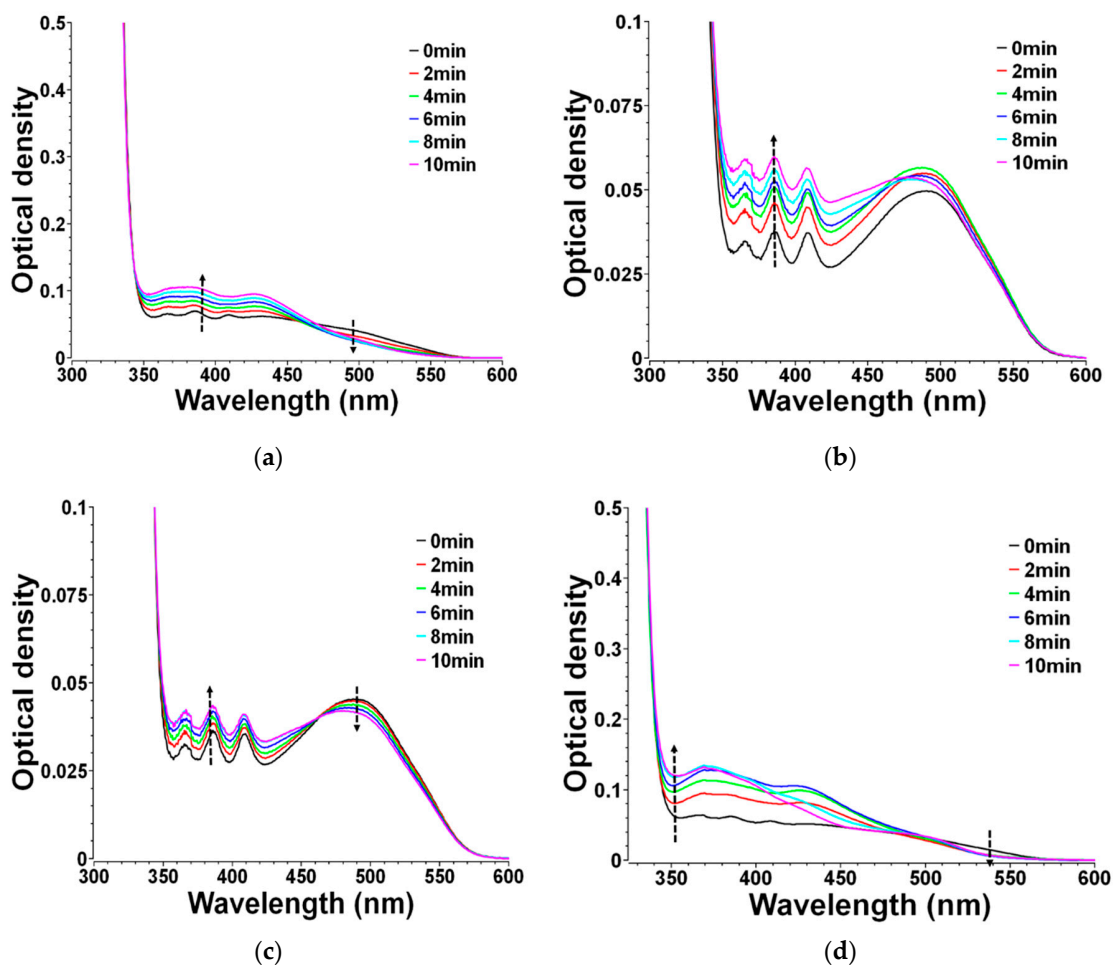
Figure 5. UV–visible absorption spectra of dye **8** (8.51×10^{-6} M in acetonitrile) with co-initiators: (**a**) iodonium salt (Iod) (1.46×10^{-4} M in acetonitrile) and amine (EDB, 4.07×10^{-4} M in acetonitrile); (**b**) Iod (Speedcure 938, 1.46×10^{-4} M in acetonitrile); (**c**) amine (EDB, 4.07×10^{-4} M in acetonitrile) upon exposure to a LED@405nm under air in acetonitrile as the solvent; (**d**) Iod (1.46×10^{-4} M in acetonitrile) and amine (EDB, 4.07×10^{-4} M in acetonitrile), sunlight, air, acetonitrile used as the solvent.

In the case of the dye **8**/Iod system, a more complex photolysis process could be evidenced, with an increase in optical density in first step, indicative of the formation of a colored photoproduct, followed by a decrease after 8 min (See Figure 5c). Additionally, the dye **8**/Iod/amine system exhibited a shoulder in the visible range (See Figure 5a) which was assigned to the formation of the colored photoproduct mentioned above.

Conversely, photolysis of dye **8**-based three-component PIS was also investigated upon irradiation with sunlight. As depicted in Figure 5d, a clear decrease in optical density was observed in the 500–550 nm range, together with an increase in optical density in the 350–500 nm range. Although an excellent photopolymerization of the monomer (TMPTA) under sunlight was observed, the photolysis speed under sunlight was greatly faster than upon irradiation with a 405 nm LED (compared to Figure 5a,d). Notably, the curve in the 375–500 nm range decreased after 8 min of irradiation, indicating the probable conversion of the new photoproducts generated during the first 8 min of irradiation to other structures and promoted by the broadness of the spectral range of sunlight.

While examining the photolysis of dye **9** in different conditions, dye **9**-based PISs also showed a fast photolysis process compared to that observed for dye **8**, which only took 5 min in solution (See Figure 6). As expected, in three-component systems, dye **9** exhibited a similar photolysis process to dye **8** resulting from their similarity in structure. However, comparison of the photolysis kinetic of

the dye **8** and **9**-based PISs in acetonitrile revealed the photolysis process to be faster for dye **9** than for dye **8** (See Figures 5 and 6, respectively). This is attributable to the higher extinction coefficients of dye **9** at 405 nm ($\varepsilon_{@405}$ = 4950 M^{-1} cm^{-1}; see Table 2), which could govern the photolysis efficiency. Indeed, dye **8** exhibits a lower molar extinction coefficient at 405 nm than dye **9** ($\varepsilon_{@405}$ = 3340 M^{-1} cm^{-1}; see Table 2).
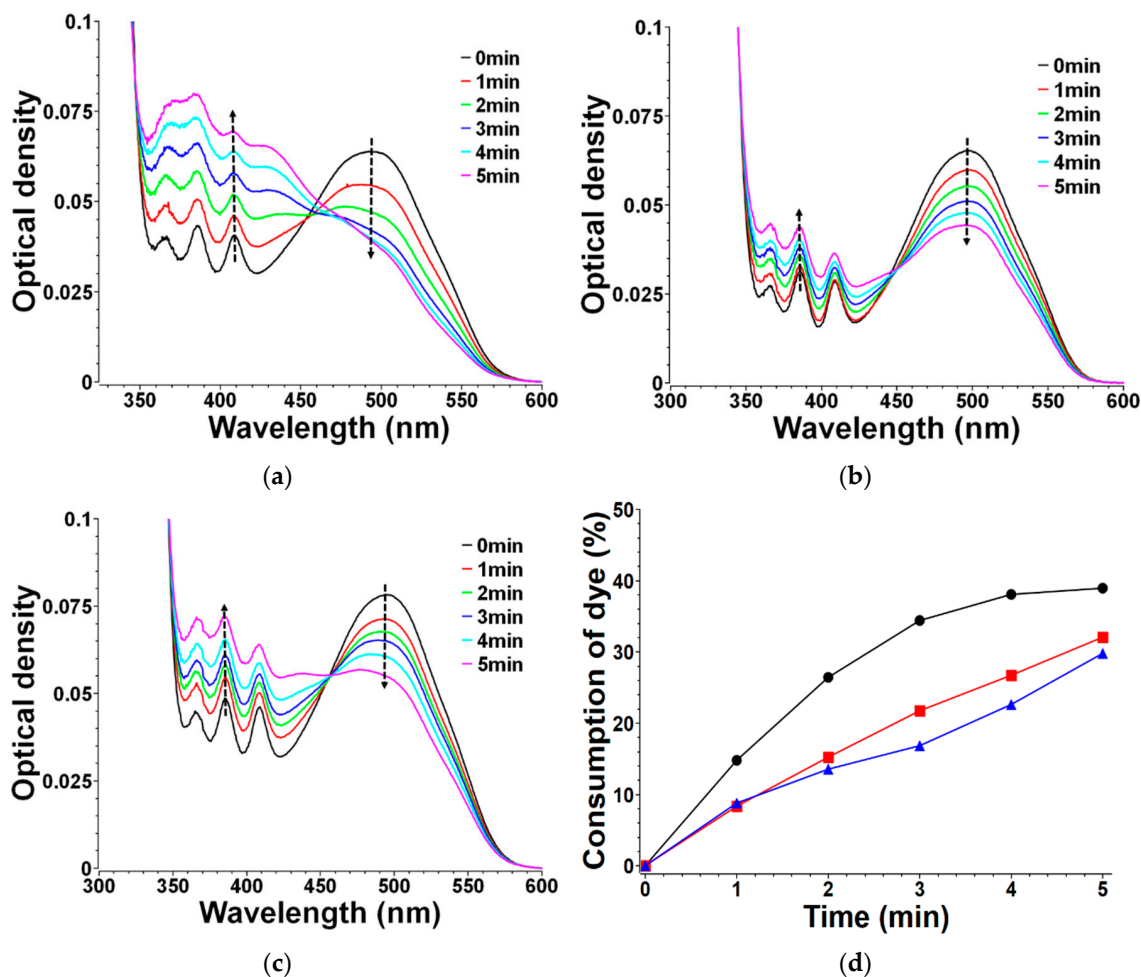

Figure 6. UV–visible absorption spectra of dye **9** (8.54×10^{-6} M in acetonitrile) with co-initiators: (**a**) Iod (1.46×10^{-4} M in acetonitrile) and amine (EDB, 4.07×10^{-4} M in acetonitrile), (**b**) Iod (1.46×10^{-4} M in acetonitrile) and (**c**) amine (EDB, 4.07×10^{-4} M in acetonitrile) upon exposure to LED@405nm under air in acetonitrile as the solvent. (**d**) Dye consumption vs. irradiation time @ λ = 405 nm: dye **9**/Iod/amine(•); dye **9**/Iod(■); dye **9**/amine(▲).

Percentage of consumption of dye **9** vs. the irradiation time can also be characterized by the changes in their respective UV–visible spectra while establishing a comparison between three-component PISs (dye/Iod/amine) and two-component PISs (dye/Iod or dye/amine). As illustrated in Figure 6d, clearly, consumption of dye **9** in the three-component PIS (dye **9**/Iod/amine) is much higher than that observed for the two-component PISs (dye **9**/Iod and dye **9**/amine combinations, e.g., the consumption of dye **9** = 38% for dye **9**/Iod/amine vs. 30% for dye **9**/Iod or 28% for dye **9**/amine). It is obvious that the two-component PIS interactions (dye **9**/Iod or dye **9**/amine) are less efficient than those observed for the three-component dye **9**/Iod/amine system.

Moreover, photolysis experiments in the presence of dye **5**, **6** and **7**-based PISs were also carried out (See Figure S1). A clear photolysis process can be observed for dyes **5**, **6** at 405 nm resulting from their high extinction coefficients at 405 nm (dye **5**: $\varepsilon_{@405}$ = 8320 M^{-1} cm^{-1}; dye **6**: $\varepsilon_{@405}$ = 22,910 M^{-1} cm^{-1};

see Table 2). Conversely, dye **7** only showed a slow photolysis process when low concentrations (dye: Iod: amine = 1.26×10^{-5} M: 1.46×10^{-4} M: 4.07×10^{-4} M) were used. Increase in the concentrations of Iod and amine in solution greatly accelerated the photolysis process. Moreover, the discussion concerning the photolysis of dye **7** can be neglected due to the low molar extinction coefficient of this dye at 405 nm ($\varepsilon_{@405}$ = 3880 M^{-1} cm^{-1}; see Figure S1c)

3.3. Laser Writing Experiments with Resins Based on Three-Component Systems and Comprising of Dye 8 or Dye 9 as Photosensitizers

Some laser writing experiments in the presence of different three-component systems dye/Iod/amine (0.1%/2%/2% w/w/w) were carried out in TMPTA in order to generate tridimensional patterns. PISs based on the three-component systems of dye **8**/Iod/amine and dye **9**/Iod/amine were selected for their remarkable performances among the eleven dyes examined in this work. The FRP of TMPTA could be initiated under mild conditions (irradiation at 405 nm), and the 3D patterns "KES" could be successfully generated (See Figure 7). The 3D patterns were obtained by efficient photopolymerization processes in a very short time and were then characterized by profilometry using a numerical optical microscope. The different patterns obtained with the dye **8**-based PIS are well-defined and exhibit 3D profiles with an excellent spatial resolution (See Figure 7a,b). Contrarily, a lower spatial resolution was observed for the 3D patterns obtained with the dye **9**-based PIS when compared to that obtained with the dye **8**-based PISs.
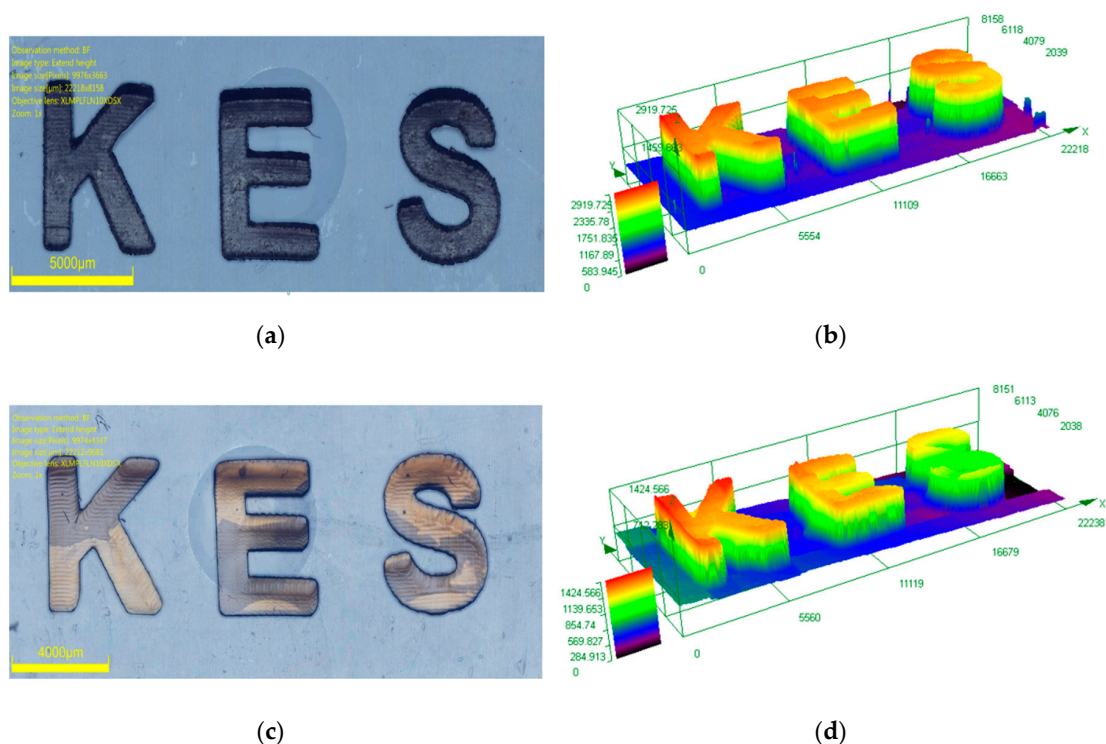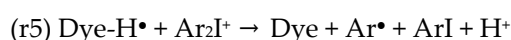

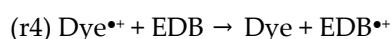(**a**)　　　　　　　　　　　　　　　　　　(**b**)

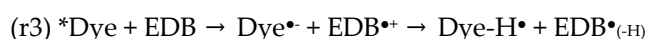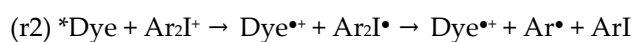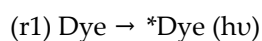(**c**)　　　　　　　　　　　　　　　　　　(**d**)

Figure 7. FRP experiments for laser writing obtained with three-component photoinitiating systems in TMPTA. Characterization by numerical optical microscopy: (**left**) top surface morphology (**right**) 3-D overall appearance of color pattern of dye/Iod/amine (0.1%/2%/2% w/w/w) in TMPTA: (**a,b**) for dye **8**/Iod/amine; (**c,d**) for dye **9**/Iod/amine.

3.4. Potential Chemical Mechanisms of Push–Pull Dyes in Photolysis Reactions

Concerning the mechanism involved in the three-component systems, plausible reactions r1, r2 and r3 presented in Scheme 5 are proposed as the chemical mechanisms occurring in the three-component dye **9**/Iod/amine system and supporting the formation of radicals (see Scheme 5). Two types of

generated radicals are proposed: (1) dye$^{\bullet+}$ and Ar$^{\bullet}$ radicals are formed upon irradiation at 405 nm by electron transfer from the excited *dye to the iodonium salt and marked as reaction r2; (2) dye-H$^{\bullet}$ is generated from *dye in the interaction of EDB and marked as reaction r3. The reactions r2 and r3 are proposed to contribute to the consumption of dyes in three-component systems. Indeed, a similar consumption is observed for the dye **9**/amine or the dye **9**/Iod combinations (See Figure 6d).

(r1) Dye → *Dye (hυ)

(r2) *Dye + Ar$_2$I$^+$ → Dye$^{\bullet+}$ + Ar$_2$I$^{\bullet}$ → Dye$^{\bullet+}$ + Ar$^{\bullet}$ + ArI

(r3) *Dye + EDB → Dye$^{\bullet-}$ + EDB$^{\bullet+}$ → Dye-H$^{\bullet}$ + EDB$^{\bullet}_{(-H)}$

(r4) Dye$^{\bullet+}$ + EDB → Dye + EDB$^{\bullet+}$

(r5) Dye-H$^{\bullet}$ + Ar$_2$I$^+$ → Dye + Ar$^{\bullet}$ + ArI + H$^+$

Scheme 5. The different steps involved in the dyes/iodonium/amine redox combination.

Similarly, the chemical mechanisms involved in the three-component dye **8**/Iod/amine combination are identical to those involved in the dye **9**/Iod/amine PIS. Conversely, no clear trend could be established concerning the consumption of dye **8** in the dye **8**/Iod two-component PIS during the irradiation process. As a rational explanation of this, the interactions between dye-H$^{\bullet}$ with Iod can also be continuously followed by reaction r5, leading to the regeneration of the dye during the aforementioned photopolymerization process.

3.5. Mechanistic Investigations in Solutions

The singlet excited state energy (E_{S1}) for the investigated dyes was calculated from the crossing point between the curve of the normalized UV–visible absorption spectra and the curve of normalized fluorescence spectra in acetonitrile (See Table 3, 2.28 eV for dye **8** and 2.38 eV for dye **9**) (See Figure 8). The free energy changes (ΔG_{Iod} = −1.22 eV, ΔG_{EDB} = 0.07 eV for dye **8**; ΔG_{Iod} = −1.36 eV, ΔG_{EDB} = −0.03 eV for dye **9**; see Table 3) for the electron transfer reactions were also investigated to examine the potential interactions between dye/Iod (or dye/amine). Additionally, the results of ΔG_{Iod} and ΔG_{EDB} for dyes **8** and **9** were calculated from the oxidation potential (E_{ox}), the reduction potential (E_{red}) and the singlet excited state energy (E_{S1}), and the oxidation potentials (or reduction potentials) of dyes **8**, **9** have been reported in the literature [5]. From the data, ΔG_{Iod} for dye **8**, ΔG_{Iod} and ΔG_{EDB} for dye **9** were less than 0, indicating the favorable interactions in dye **8**/Iod, dye **9**/Iod and dye **9**/amine systems. Thus, the interactions will also be investigated by fluorescence quenching in the following context.

Table 3. Parameters characterizing the chemical mechanisms associated with dyes **8** and **9** in acetonitrile [a].

	E_{S1} (eV)	E_{red} (eV) [b]	E_{ox} (eV) [b]	ΔG^{S1}_{Iod} [a] (eV) [d]	ΔG^{S1}_{EDB} (eV) [d]
Dye **8**	2.28	−1.35	0.36	−1.22	0.07
Dye **9**	2.38	−1.41	0.32	−1.36	−0.03
	E_{T1} (eV) [c]	$\Delta G_{et}{}^{T1}_{Iod}$ (eV) [d]	$\Delta G_{et}{}^{T1}_{EDB}$ (eV) [d]	$K^{sv(S1)}_{EDB}$ (M^{-1})	$\phi^{et(S1)}_{EDB}$ [a]
Dye **8**	1.65	−0.59	0.7	-	-
Dye **9**	1.65	−0.63	0.76	129	0.937

[a]: A re-evaluated value of reduction potential of −0.7 V is used according to [38]; [b]: from the values presented in [5]; [c]: calculated triplet state energy level at Density Functional Theory (DFT) level; [d]: from the equation presented in [39].
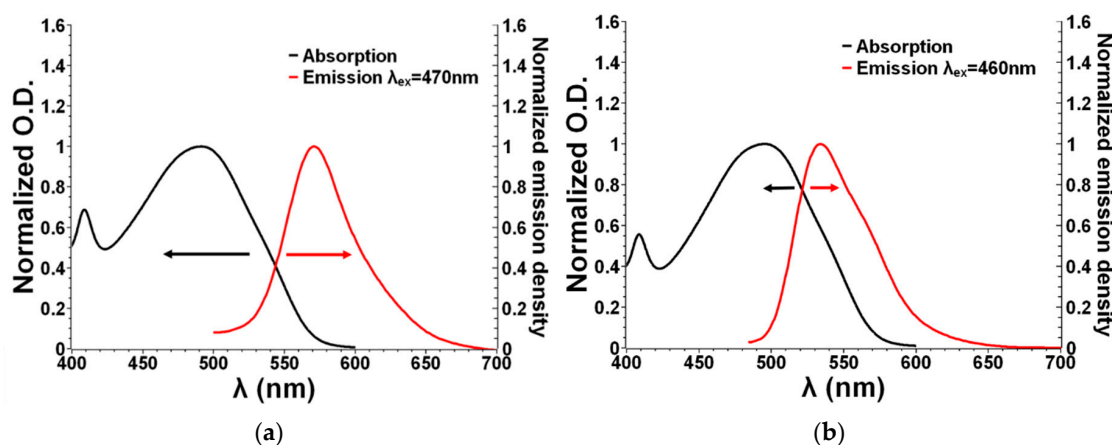
Figure 8. Singlet state energy determination in acetonitrile for (**a**) dye **8** and (**b**) dye **9**.

Triplet energy levels for dyes **8** and **9** were also calculated, and the results are shown in Table 3. A mechanism involving the triplet state cannot be excluded for the dye/iodonium interaction ($\Delta G < 0$; Table 3). Conversely, the triplet route can be excluded for the dye/amine combination ($\Delta G > 0$; see Table 3).

The fluorescence quenching experiments were performed in acetonitrile (Figure 9). For the dye **8**/EDB system, no fluorescence quenching was observed in acetonitrile. A linear quenching process was observed for the dye **9**/EDB combination, and its Stern–Volmer coefficients (Ksv = 129 M^{-1} for dye **9**/EDB; Table 3) and the electron transfer quantum yields (ϕet; Table 3) were also determined. Interestingly, dye **8** (or dye **9**)/Iod interaction showed an increasing tendency, which indicates that new photoproducts are generated (See Figure S2). These results are in full agreement with the highly favorable free energy changes (ΔGet(Dye/EDB)) for the electron transfer reaction between dyes and EDB (or Iod).

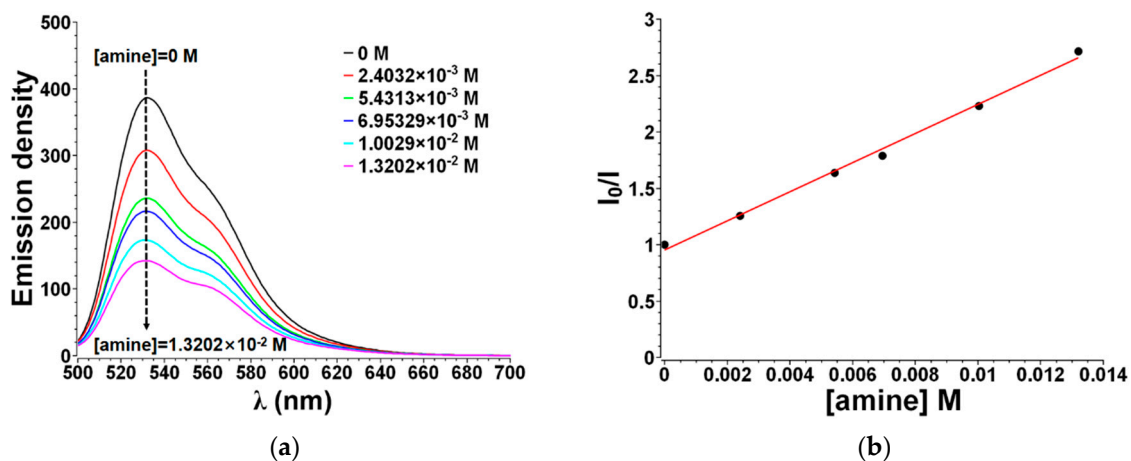**Figure 9.** (**a**) Fluorescence quenching of dye **9** (8.54×10^{-6} M in acetonitrile) by amine (Speedcure EDB); (**b**) Stern−Volmer treatment for the dye **9**/amine fluorescence quenching.

3.6. ESR Spin-Trapping Experiments

To demonstrate the chemical mechanisms of the push–pull dye-initiated photopolymerization, ESR spin trapping experiments were carried out by irradiating at 405 nm with an LED, and some radicals were detected after mixing of dye **8**/Iod and dye **8**/amine in *tert*-butylbenzene under inert atmosphere in the presence of a spin trap agent (PBN). The PBN/Ar• adduct was detected, and the following hyperfine coupling constants (hfc) constants could be determined by simulation: a$_N$ = 14.38 G and

a_H = 2.15 G for the dye **8**/Iod PIS. The PBN/ArNCH$_3$CH$_2\bullet$ adduct was also detected, and values of a_N = 14.38 G and a_H = 2.14 G for the dye **8**/amine PIS (see Figure 10) could be calculated, which fully match to the literature [40].
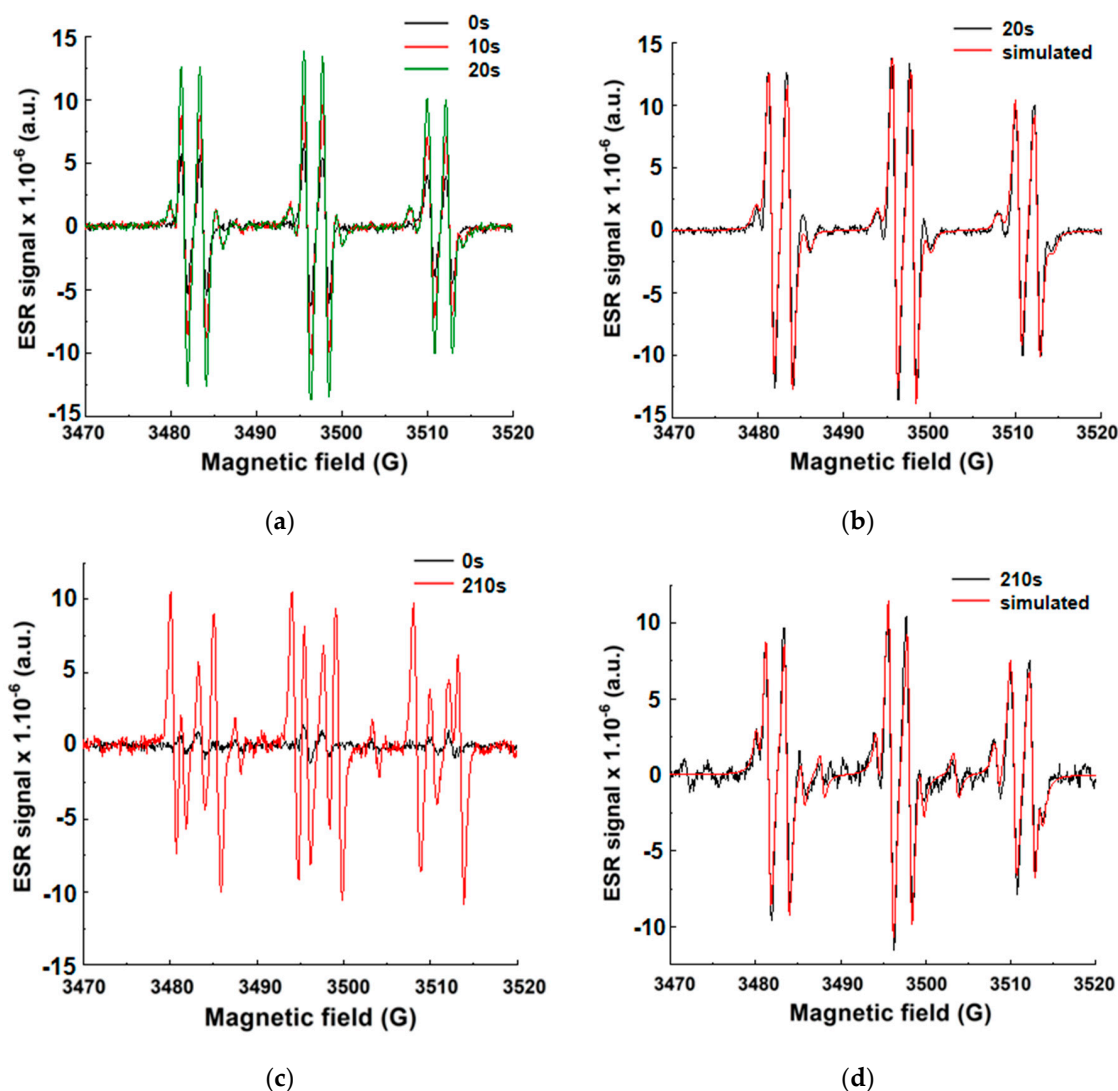

Figure 10. Electron spin resonance (ESR) spectra obtained from the ESR spin-trapping experiment using presence of a spin trap agent (PBN) = 2 mg/mL (as spin trap agent); iodonium salt = 12.6 mg/mL; and dye **8** = 0.8 mg/mL in *tert*-butylbenzene under N$_2$. (**a**) Dye **8**/Iod photoinitiating system (PIS), irradiation time = 20 s (green), = 10 s (red) and = 0 s (black) spectra, respectively; (**b**) dye 8/Iod PIS, irradiation time = 20 s (black) and simulated (red) spectra; (**c**) **dye 8/amine PIS**, irradiation time = 210 s (red) and = 0 s (black) spectra; (**d**) **dye 8/amine PIS**, irradiation time = 210 s (black) and simulated (red) spectra.

The dye **9**/Iod and dye **9**/amine solutions in *tert*-butylbenzene under inert atmosphere and in the presence of PBN were also characterized by ESR spin-trapping experiments upon irradiation at 405 nm with a LED. As expected, the two radical adducts PBN/Ar$\bullet$ and PBN/ArNCH$_3$CH$_2\bullet$ were also detected and characterized by a_N = 14.39 G; a_H = 2.14 G and a_N = 14.41 G; a_H = 2.17 G (dye **9**/Iod and dye **9**/amine PISs, respectively—see Figure S3), which is in agreement with the literature. Therefore, it can be concluded that the ESR experiments perfectly fit with the mechanism proposed in the Scheme 3 [41].

3.7. Laser Writing Experiments for the Photocomposites Prepared by Push–Pull Dye-Based PISs and Silica Fillers

Photocomposites were prepared with the dye **8** or **9**/Iod/amine three-component systems (0.1:2:2 in monomer, w/w/w), and silica was added as filler (20% in monomer, w/w) for a TMPTA-based resin. Laser writing experiments were carried out with the prepared photocurable resins. The 3D patterns obtained after irradiation were examined by profilometry with a numerical optical microscope (Figure 11). As a result, laser writing experiments carried out on these filled photocomposites comprising dyes **8** or **9**, and a lower spatial resolution was observed for the different 3D patterns when compared to those obtained with the dye **8** or **9** PISs for resins without fillers. This can be attributed to a lower light penetration when fillers are incorporated in the photocurable resins. However, dyes **8** or **9** also presented a relatively remarkable reactivity in the presence of fillers. The quality of the 3D structures obtained with and without fillers clearly demonstrates the full potential of the new photoinitiating systems proposed in this work for the fabrication of photopolymerizable materials in the future.
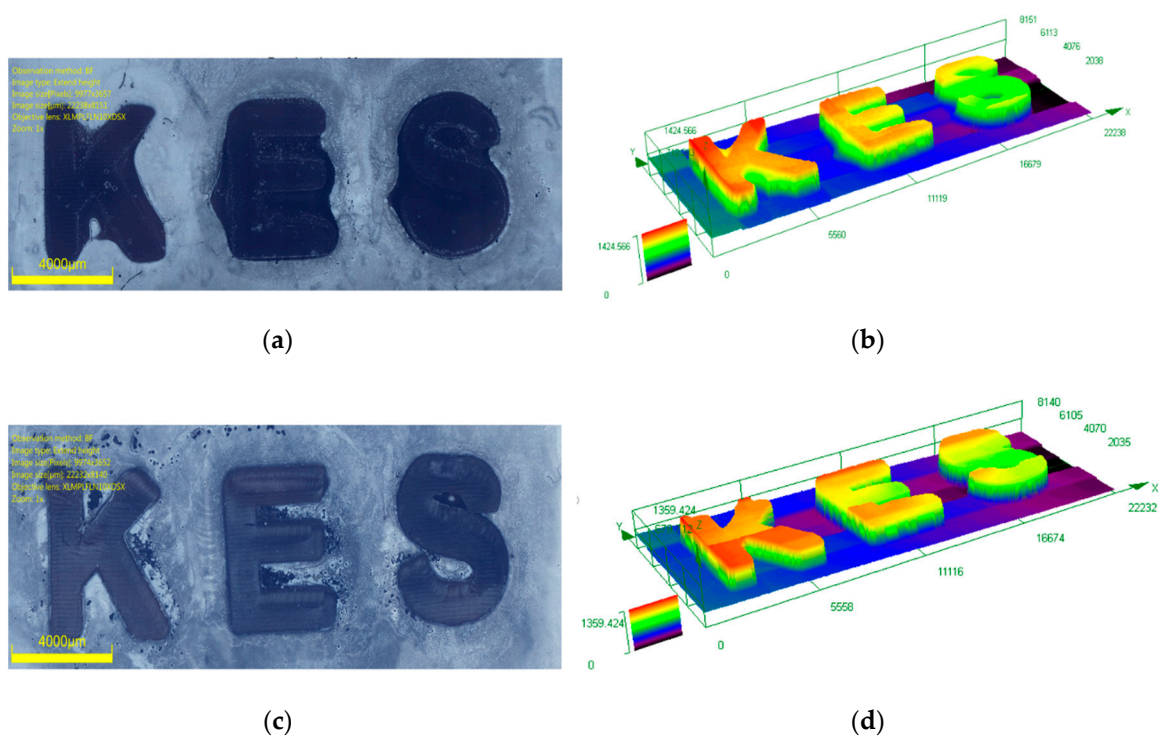

(**a**)   (**b**)

(**c**)   (**d**)

Figure 11. Free radical photopolymerization experiments for laser writing initiated by dye-based three-component photoinitiating systems in TMPTA. Characterization of the 3D patterns by numerical optical microscopy: (**left**) top surface morphology (**right**), 3D overall appearance of color pattern of dye/Iod/amine (0.1%/2%/2% w/w/w) in TMPTA (**a,b**) for dye **8**/Iod/amine (0.1%/2%/2% w/w/w) in the presence of silica (20%, w/w) in TMPTA; (**c,d**) for dye **9**/Iod/amine (0.1%/2%/2% w/w/w) in the presence of silica (20%, w/w) in TMPTA.

4. Materials and Methods

4.1. Dyes

Dyes **1–11** investigated in this article were synthesized with high purity as reported in supplementary information. Chemical structures are given in Figure 1.

4.2. Other Materials

Chemicals including the iodonium salt (Iod; also noted Speedcure 938) and the amine (ethyl dimethylaminobenzoate (EDB) were purchased from Lambson Ltd. (Wetherby, UK), and the photopolymerizable monomer (TMPTA) was obtained from Allnex (Frankfurt, Germany) (See structures in Scheme 2). Particularly, to highlight the potential applications of these dyes in green chemistry, all photopolymerization processes were performed in solvent-free and mild conditions e.g., at room temperature.

4.3. Photopolymerization Experiments

Photoinitiating systems used in this work are composed of a dye, iodonium salt (Iod) and the amine (EDB) and are exposed to an LED@405 nm ($I_0 = 110$ mW cm^{-2}) in ambient conditions and under air. In detail, their weight contents (kept at 0.1w%/2%/2% w/w/w, respectively) were calculated from the monomer (TMPTA) content, and the different polymerization experiments were carried out in laminate (the monomer thickness was controlled).

Monitoring of the reaction was performed as previously reported [42–44]. The conversion of the acrylate functions at a given time is calculated as

$$\text{conversion (\%)} = (A_0 - A_t)/A_0 \times 100 \tag{1}$$

where A_0 is the initial peak area before irradiation, and A_t is the peak area after irradiation for a given time t [45].

4.4. UV–Visible Absorption, Photolysis and Fluorescent Properties

These different experiments were carried out with equipment and experimental conditions reported in previous works [46,47].

4.5. Redox Potentials

The redox potentials of dyes **8** and **9** (oxidation potential noted E_{ox} and reduction potential noted E_{red}) were reported in [5]. The dyes were dispersed in acetonitrile while using tetrabutylammonium hexafluorophosphate as the supporting electrolyte (potential vs. Saturated Calomel Electrode, SCE). The excited state energy level noted $E^*(Es_1)$ was determined from the crossing point of the absorption and photoluminescence spectra. Thus, the free energy change of the singlet state ΔG^{S1}_{Iod} or ΔG^{S1}_{EDB} for the electron transfer reaction was determined by E_{ox}, E_{red}, and $E^*(Es_1)$ which were calculated from Equations (2) and (3) [48]. Similarly, the free energy change of triplet state ΔG_{et} was calculated by E_{ox}, E_{red}, and $E^*(E_{T1})$ from the Equations (4) and (5) (Equations (4) and (5)) [46], where the triplet state energy level (noted $E^*(E_{T1})$) was extracted from molecular energy level calculations (Gaussian 03 suite of programs). The reduction potential of iodonium was −0.7 V, and the oxidation potential of EDB was +1.0 V [38,39].

$$\Delta G^{S1}_{Iod} = E_{ox} - (-0.7) - E^* (E_{S1}) \tag{2}$$

$$\Delta G^{S1}_{EDB} = 1 - (E_{red}) - E^* (E_{S1}) \tag{3}$$

$$\Delta G^{et}_{Iod} = E_{ox} - (-0.7) - E^* (E_{T1}) \tag{4}$$

$$\Delta G^{et}_{EDB} = 1 - (E_{red}) - E^* (E_{T1}) \tag{5}$$

4.6. Preparation of Photocomposites

Photocomposites were prepared from dye/iodonium salts (Iod)/amine (EDB) systems and fillers of silica. Their weight contents kept at dye/Iod/amine/silica = 0.1%/2%/2%/20%, w/w/w/w were calculated from the monomer (TMPTA) content at room temperature and under air.

4.7. 3D Printing Experiments

3D printing experiments were carried out in conditions previously detailed [49,50].

4.8. Electron Spin Resonance (ESR) Spin Trapping (ESR-ST)

Electron spin resonance spin-trapping experiments were carried out in conditions previously detailed [44,51]. Simulations were carried out using PEST WINSIM software.

4.9. Computational Procedure

The triplet state energies were calculated at the UB3LYP/6-31G* level. Geometries were frequency checked [52,53].

5. Conclusions

In summary, eleven new dyes based on a push–pull structure were synthesized for the design of new photoinitiating systems when combined with an iodonium salt and an amine to initiate the FRP of a highly reactive acrylate (TMPTA) resin. Among the different dyes, two dyes with 3-(dialkylamino)-1,2-dihydro-9-oxo-9*H*-indeno [2,1-*c*] pyridine-4-carbonitrile group were selected as the most representative photoinitiators. The different complementary experiments done in order to determine the photochemical mechanism were thus conducted on these two candidates. Notably, the steady-state photolysis and fluorescence quenching of the dye-based photoinitiating systems were observed by UV–visible experiments and fluorescence approaches. Moreover, the proposed chemical mechanisms have been investigated and discussed by free energy change calculations. The generated free radicals were detected by ESR experiments, which also confirmed the proposed chemical mechanisms. Interestingly, among the remarkable light absorption properties, their exceptional photochemical reactivity enabled the design of highly efficient photoinitiating systems with these dyes. Remarkably, due to their huge performance, sunlight-induced polymerization is possible.

Finally, 3D patterns were generated by dyes **8** and **9**-based three-component photoinitiating systems, and the photocomposites were fabricated by filling silica. Comparison between these 3D patterns obtained with and without fillers was also discussed. Overall, this research contributes to improving the knowledge concerning the use of push–pull chromophores as photoinitiators of polymerization. Interestingly, if 1*H*-cyclopentanaphthalene-1,3-dione has only been scarcely used to elaborate push–pull dyes, the results obtained in this work clearly demonstrate the full potential of this unusual electron acceptor for the design of push–pull dyes, and its deserves to be more widely used in the future, not just for the design of photoinitiators but more generally in all research fields making use of push–pull dyes.

References

1. Bures, F. Fundamental aspects of property tuning in push–pull molecules. *RSC Adv.* **2014**, *4*, 58826–58851. [CrossRef]

2. Pigot, C.; Noirbent, G.; Peralta, S.; Duval, S.; Nechab, M.; Gigmes, D.; Dumur, F. Unprecedented Nucleophilic Attack of Piperidine on the Electron Acceptor during the Synthesis of Push-Pull Dyes by a Knoevenagel Reaction. *Helv. Chim. Acta* **2019**, *102*, e1900229. [CrossRef]

3. Guda, R.; Bhaskar, A.; Goodson, T. Ultrafast excited state relaxation dynamics of branched donor-π-acceptor chromophore: Evidence of a charge-delocalized state. *J. Phys. Chem. B* **2006**, *110*, 20872–20878.

4. Kivala, M.; Diederich, F. Acetylene-derived strong organic acceptors for planar and nonplanar push– pull chromophores. *Acc. Chem. Res.* **2019**, *42*, 235–248. [CrossRef]

5. Pigot, C.; Noirbent, G.; Peralta, S.; Duval, S.; Bui, T.T.; Aubert, P.H.; Nechab, M.; Gigmes, D.; Dumur, F. New push-pull dyes based on 2-(3-oxo-2,3-dihydro-1*H*-cyclopenta[*b*]naphthalen-1-ylidene) malononitrile: An amine-directed synthesis. *Dyes Pigment.* **2020**, *175*, 108182. [CrossRef]

6. Paek, S.; Lee, J.K.; Ko, J. Synthesis and photovoltaic characteristics of push–pull organic semiconductors containing an electron-rich dithienosilole bridge for solution-processed small-molecule organic solar cells. *Sol. Energy Mater. Solar Cells* **2014**, *120*, 209–217. [CrossRef]

7. Xu, S.J.; Zhou, Z.; Liu, W.; Zhang, Z.; Liu, F.; Yan, H.; Zhu, X. A twisted thieno[3,4-*b*]thiophene-based electron acceptor featuring a 14-π-electron indenoindene core for high-performance organic photovoltaics. *Adv. Mater.* **2017**, *29*, 1704510. [CrossRef] [PubMed]

8. Turkoglu, G.; Cinar, M.E.; Ozturk, T. Triarylborane-based materials for OLED applications. *Molecules* **2017**, *22*, 1522. [CrossRef] [PubMed]

9. Karak, S.; Liu, F.; Russell, T.P.; Duzhko, V.V. Bulk charge carrier transport in push-pull type organic semiconductor. *ACS Appl. Mater. Interfaces* **2014**, *6*, 20904–20912. [CrossRef]

10. Raimundo, J.M.; Blanchard, P.; Gallego-Planas, N.; Mercier, N.; Ledoux-Rak, I.; Hierle, R.; Roncali, J. Design and synthesis of push-pull chromophores for second-order nonlinear optics derived from rigidified thiophene-based π-conjugating spacers. *J. Org. Chem.* **2002**, *67*, 205–218. [CrossRef]

11. El-Shishtawy, R.M.; Borbone, F.; Al-Amshany, Z.M.; Tuzi, A.; Barsella, A.; Asiri, A.M.; Roviello, A. Thiazole azo dyes with lateral donor branch: Synthesis, structure and second order NLO properties. *Dyes Pigment.* **2013**, *96*, 45–51. [CrossRef]

12. Cesaretti, A.; Bonaccorso, C.; Elisei, F.; Fortuna, C.G.; Mencaroni, L.; Spalletti, A. Photoinduced intramolecular charge transfer and hyperpolarizability coefficient in push-pull pyridinium salts with increasing strength of the acceptor group. *ChemPlusChem* **2018**, *83*, 1021–1031. [CrossRef] [PubMed]

13. Motiei, H.; Jafari, A.; Naderali, R. Third-order nonlinear optical properties of organic azo dyes by using strength of nonlinearity parameter and Z-scan technique. *Opt. Laser Technol.* **2017**, *88*, 68–74. [CrossRef]

14. El-Shishtawy, R.M.; Al-Zahrani, F.A.; Afzal, S.M.; Razvi, M.A.N.; Al-Amshany, Z.M.; Bakry, A.H.; Asiri, A.M. Synthesis, linear and nonlinear optical properties of a new dimethine cyanine dye derived from phenothiazine. *RSC Adv.* **2016**, *6*, 91546–91556. [CrossRef]

15. Chaumel, F.; Jiang, H.; Kakkar, A. Sol−gel materials for second-order nonlinear optics. *Chem. Mater.* **2001**, *13*, 3389–3395. [CrossRef]

16. Matsumoto, S.; Kubodera, K.I.; Kurihara, T.; Kaino, T. Nonlinear optical properties of an azo dye attached polymer. *Appl. Phys. Lett.* **1987**, *51*, 1–2. [CrossRef]

17. Gao, S.H.; Xie, M.S.; Wang, H.X.; Niu, H.Y.; Qu, G.R.; Guo, H.M. Highly selective detection of Hg^{2+} ion by push–pull-type purine nucleoside-based fluorescent sensor. *Tetrahedron* **2014**, *70*, 4929–4933. [CrossRef]

18. Kim, E.; Felouat, A.; Zaborova, E.; Ribierre, J.C.; Wu, J.W.; Senatore, S.; Matthews, C.; Lenne, P.F.; Baffert, C.; Karapetyan, A.; et al. Boron difluoride complexes of hemicurcuminoids as bio-inspired push–pull dyes for bioimaging. *Org. Biomol. Chem.* **2016**, *14*, 1311–1324. [CrossRef]

19. Li, C.; Plamont, M.A.; Aujard, I.; Le Saux, T.; Jullien, L.; Gautier, A. Design and characterization of red fluorogenic push–pull chromophores holding great potential for bioimaging and biosensing. *Org. Biomol. Chem.* **2016**, *14*, 9253–9261. [CrossRef]

20. Noirbent, G.; Dumur, F. Recent advances on nitrofluorene derivatives: Versatile electron acceptors to create dyes absorbing from the visible to the near and far-infrared region. *Materials* **2018**, *11*, 2425. [CrossRef]

21. Blanchard-Desce, M.; Wortmann, R.; Lebus, S.; Lehn, J.M.; Krämer, P. Intramolecular charge transfer in elongated donor-acceptor conjugated polyenes. *Chem. Phys. Lett.* **1995**, *243*, 526–532. [CrossRef]

22. Noirbent, G.; Pigot, C.; Bui, T.-T.; Péralta, S.; Nechab, M.; Gigmes, D.; Dumur, F. Synthesis, optical and electrochemical properties of a series of push-pull dyes based on the 2-(3-cyano-4,5,5-trimethylfuran-2(5H)-ylidene) malononitrile (TCF) acceptor. *Dyes Pigment.* **2021**, *184*, 108807. [CrossRef]

23. Tehfe, M.-A.; Dumur, F.; Graff, B.; Morlet-Savary, F.; Gigmes, D.; Fouassier, J.-P.; Lalevée, J. Push-pull (thio)barbituric acid derivatives in dye photosensitized radical and cationic polymerization reactions under 457/473 nm Laser beams or blue LEDs. *Polym. Chem.* **2013**, *4*, 3866–3875. [CrossRef]

24. Dumur, F.; Gigmes, D.; Fouassier, J.-P.; Lalevée, J. Organic Electronics: An El Dorado in the quest of new photoCatalysts as photoinitiators of polymerization. *Acc. Chem. Res.* **2016**, *49*, 1980–1989. [CrossRef] [PubMed]

25. Tehfe, M.A.; Dumur, F.; Graff, B.; Morlet-Savary, F.; Gigmes, D.; Fouassier, J.P.; Lalevée, J. New push-pull dyes derived from Michler's ketone for polymerization reactions upon visible lights. *Macromolecules* **2013**, *46*, 3761–3770. [CrossRef]

26. Xiao, P.; Frigoli, M.; Dumur, F.; Graff, B.; Gigmes, D.; Fouassier, J.P.; Lalevée, J. Julolidine or fluorenone based push-pull dyes for polymerization upon soft polychromatic visible light or green light. *Macromolecules* **2014**, *47*, 106–112. [CrossRef]

27. Tehfe, M.-A.; Dumur, F.; Graff, B.; Gigmes, D.; Fouassier, J.-P.; Lalevée, J. Blue-to-red light sensitive push-pull structured photoinitiators: Indanedione derivatives for radical and cationic photopolymerization reactions. *Macromolecules* **2013**, *46*, 3332–3341. [CrossRef]

28. Mokbel, H.; Telitel, S.; Dumur, F.; Vidal, L.; Versace, D.-L.; Tehfe, M.-A.; Graff, B.; Toufaily, J.; Fouassier, J.-P.; Gigmes, D.; et al. Photoinitiating systems of polymerization and in-situ incorporation of metal nanoparticles in polymer matrixes upon visible lights: Push-pull malonate and malonitrile based dyes. *Polym. Chem.* **2013**, *4*, 5679–5687. [CrossRef]

29. Sun, K.; Xu, Y.; Dumur, F.; Morlet-Savary, F.; Chen, H.; Dietlin, C.; Graff, B.; Lalevée, J.; Xiao, P. In silico rational design by molecular modeling of new ketones as photoinitiators in three-component photoinitiating systems: Application in 3D printing. *Polym. Chem.* **2020**, *11*, 2230–2242. [CrossRef]

30. Liu, S.; Brunel, D.; Sun, K.; Xu, Y.; Morlet-Savary, F.; Graff, B.; Xiao, P.; Dumur, F.; Lalevée, J. A Monocomponent bifunctional benzophenone-carbazole type II photoinitiator for led photoinitiating systems. *Polym. Chem.* **2020**, *11*, 3551–3556. [CrossRef]

31. Chen, H.; Noirbent, G.; Sun, K.; Brunel, D.; Gigmes, D.; Morlet-Savary, F.; Zhang, Y.; Liu, S.; Xiao, P.; Dumur, F.; et al. Photoinitiators derived from natural product scaffolds: Monochalcones in three-component photoinitiating systems and their applications in 3D printing. *Polym. Chem.* **2020**, *11*, 4647–4659. [CrossRef]

32. Liu, S.; Chen, H.; Zhang, Y.; Sun, K.; Xu, Y.; Morlet-Savary, F.; Graff, B.; Noirbent, G.; Pigot, C.; Brunel, D.; et al. Monocomponent photoinitiators based on benzophenone-carbazole structure for led photoinitiating systems and application on 3D printing. *Polymers* **2020**, *12*, 1394. [CrossRef] [PubMed]

33. Xu, Y.; Noirbent, G.; Brunel, D.; Liu, F.; Gigmes, D.; Sun, K.; Zhang, Y.; Liu, S.; Morlet-Savary, F.; Xiao, P.; et al. Ketone derivatives as photoinitiators for both radical and cationic photopolymerizations under visible LED and application in 3D printing. *Eur. Polym. J.* **2020**, *132*, 109737. [CrossRef]

34. Pigot, C.; Noirbent, G.; Bui, T.T.; Péralta, S.; Gigmes, D.; Nechab, M.; Dumur, F. Push-pull chromophores based on the naphthalene scaffold: Potential candidates for optoelectronic applications. *Materials* **2019**, *12*, 1342. [CrossRef]

35. Sun, K.; Pigot, C.; Chen, H.; Nechab, M.; Gigmes, D.; Morlet-Savary, F.; Graff, B.; Liu, S.; Xiao, P.; Dumur, F.; et al. Free radical photopolymerization and 3D printing using newly developed dyes: Indane-1, 3-dione and 1H-cyclopentanaphthalene-1, 3-dione derivatives as photoinitiators in three-component systems. *Catalysts* **2020**, *10*, 463. [CrossRef]

36. Pigot, C.; Noirbent, G.; Brunel, D.; Dumur, F. Recent advances on push-pull organic dyes as visible light photoinitiators of polymerization. *Eur. Polym. J.* **2020**, *133*, 109797. [CrossRef]

37. Landmesser, T.; Linden, A.; Hansen, H.J. A Novel Route to 1-Substituted 3-(Dialkylamino)-9-Oxo-9H-Indeno[2,1-c]Pyridine-4-Carbonitriles. *Helv. Chim. Acta* **2008**, *91*, 265–284. [CrossRef]

38. Romanczyk, P.P.; Kurek, S.S. The Reduction Potential of Diphenyliodonium Polymerisation Photoinitiator Is Not −0.2 V vs. SCE. A Computational Study. *Electrochim. Acta* **2017**, *225*, 482–485. [CrossRef]

39. Fouassier, J.P.; Lalevée, J. *Photoinitiators for Polymer Synthesis—scope, Reactivity, and Efficiency*; John Wiley Sons: Weinheim, Germany, 2012.

40. Haire, L.D.; Krygsman, P.H.; Janzen, E.G.; Oehler, U.M. Correlation of radical structure with EPR spin adduct parameters: Utility of the proton, carbon-13, and nitrogen-14 hyperfine splitting constants of aminoxyl adducts of PBN-nitronyl-^{13}C for three-parameter scatter plots. *J. Org. Chem.* **1988**, *53*, 4535–4542. [CrossRef]

41. Ohto, N.; Niki, E.; Kamiya, Y. Study of autoxidation by spin trapping. Spin trapping of peroxyl radicals by phenyl *N*-t-butyl nitrone. *J. Chem. Soc. Perkin Trans. 2* **1977**, *13*, 1770–1774. [CrossRef]

42. Dietlin, C.; Schweizer, S.; Xiao, P.; Zhang, J.; Morlet-savary, F.; Graff, B.; Fouassier, J.P.; Lalevée, J. Photopolymerization upon LEDs: New photoinitiating systems and strategies. *Polym. Chem.* **2015**, *6*, 3895–3912. [CrossRef]

43. Lalevée, J.; Blanchard, N.; Tehfe, M.A.; Morlet-Savary, F.; Fouassier, J.P. Green bulb light source induced epoxy cationic polymerization under air using tris (2, 2′-bipyridine) ruthenium (II) and silyl radicals. *Macromolecules* **2010**, *43*, 10191–10195. [CrossRef]

44. Lalevée, J.; Blanchard, N.; Tehfe, M.A.; Peter, M.; Morlet- Savary, F.; Gigmes, D.; Fouassier, J.P. Efficient dual radical/cationic photoinitiator under visible light: A new concept. *Polym. Chem.* **2011**, *2*, 1986–1991. [CrossRef]

45. Xu, Y.Y.; Ding, Z.F.; Liu, F.Y.; Sun, K.; Dietlin, C.; Lalevée, J.; Xiao, P. 3D Printing of Polydiacetylene Photocomposite Materials: Two Wavelengths for Two Orthogonal Chemistries. *ACS Appl. Mater. Interf.* **2019**, *12*, 1658–1664. [CrossRef] [PubMed]

46. Abdallah, M.; Hijazi, A.; Graff, B.; Fouassier, J.-P.; Rodeghiero, G.; Gualandi, A.; Dumur, F.; Cozzi, P.G.; Lalevée, J. Coumarin derivatives as versatile photoinitiators for 3D printing, polymerization in water and photocomposite synthesis. *Polym. Chem.* **2019**, *10*, 872–884. [CrossRef]

47. Abdallah, M.; Bui, T.-T.; Goubard, F.; Theodosopoulou, D.; Dumur, F.; Hijazi, A.; Fouassier, J.-P.; Lalevée, J. Phenothiazine derivatives as photoredox catalysts for cationic and radical photosensitive resins for 3D printing technology and photocomposite synthesis. *Polym. Chem.* **2019**, *10*, 6145–6156. [CrossRef]

48. Rehm, D.; Weller, A. Kinetics of fluorescence quenching by electron and H-atom transfer. *Isr. J. Chem.* **1970**, *8*, 259–271. [CrossRef]

49. Zhang, J.; Dumur, F.; Xiao, P.; Graff, B.; Bardelang, D.; Gigmes, D.; Fouassier, J.P.; Lalevée, J. Structure design of naphthalimide derivatives: Toward versatile photoinitiators for near-UV/visible LEDs, 3D printing, and water-soluble photoinitiating systems. *Macromolecules* **2015**, *48*, 2054–2063. [CrossRef]

50. Xiao, P.; Dumur, F.; Zhang, J.; Fouassier, J.-P.; Gigmes, D.; Lalevée, J. Copper complexes in radical photoinitiating systems: Applications to free radical and cationic polymerization upon visible LEDs. *Macromolecules* **2014**, *47*, 3837–3844. [CrossRef]

51. Telitel, S.; Dumur, F.; Campolo, D.; Poly, J.; Gigmes, D.; Fouassier, J.-P.; Lalevée, J. Iron complexes as potential photocatalysts for controlled radical photopolymerizations: A tool for modifications and patterning of surfaces. *J. Polym. Sci. A Polym. Chem.* **2016**, *54*, 702–713. [CrossRef]

52. James, B.; Frisch, A. *Exploring Chemistry with Electronic Structure Methods*; Gaussian Inc.: Wallingford, CT, USA, 1996.

53. Frisch, M.J.; Trucks, G.W.; Schlegel, H.B.; Scuseria, G.E.; Robb, M.A.; Cheeseman, J.R.; Zakrzewski, V.G.; Montgomery, J.A.; Stratmann, R.E.; Burant, J.C.; et al. *Gaussian 03, Revision B-2*; Gaussian Inc.: Pittsburgh, PA, USA, 2003.